



46 On the other hand, representing the span and the variability in time and space of the dust aerosol size
47 distribution remains a challenge.

48 The particle size distribution of mineral dust extends over several order of magnitudes. Iron-rich
49 particles as small as 14 nm in diameter have been observed in the laboratory from deflating soils by
50 Baddock et al. (2013). During sandstorm in Algeria, Gomes et al. (1990) measured an increase of the
51 mass concentration of particles between 100 nm and 1 μm , and attributed to clays disaggregated by
52 sandblasting. Measurements of the size-resolved vertical dust flux by Gillette et al. (1972; 1974a;
53 1974b) based on microscopy analyses of samples from Texas and Nebraska showed the presence of
54 particles up to several microns in dust emissions.

55 The representation of the accumulation and coarse modes in mineral dust has long being based on the
56 columnar measurements by the sun/sky photometers of the Aerosol Robotic Network (AERONET)
57 network, which provides with normalized size distributions of mineral dust considered as chemically
58 homogeneous particles the 0.1–30 μm optically-equivalent diameter (Dubovik et al., 2002; 2006;
59 Holben et al., 2011), and which, incidentally, serve also the look-up tables of the remote sensing
60 retrievals of dust from space (e.g., Cuesta et al., 2015; Zhou et al., 2020).

61 Nevertheless, in situ observations at ground-based stations and on aircraft in more recent years have
62 shown that particles of several tenths, sometimes hundreds, of micron are airborne at emission, and
63 remain so after several days of transport (Reid et al., 2003; Formenti et al., 2003; Rajot et al., 2008;
64 Chou et al., 2008; Kandler et al., 2007; 2009; Wagner et al., 2009; Klaver et al., 2011; Ryder et al., 2013;
65 2015; Rosenberg et al., 2014; Denjean et al., 2016; Wienzerl et al., 2017; van der Does et al., 2018).

66 These observations have been instrumental to a number of advances. Using them as ensemble dataset,
67 to smooth spurious atmospheric variability, they have served as a basis to a new classification of the
68 dust size distribution in four modes, namely fine dust (diameter $\leq 2.5 \mu\text{m}$), coarse dust ($2.5 < \text{diameter}$
69 $\leq 10 \mu\text{m}$), super coarse dust ($10 < \text{diameter} \leq 62.5 \mu\text{m}$) and giant dust (diameter $> 62.5 \mu\text{m}$), extending
70 above the size range retrieved by AERONET (Adeyemi et al., 2023). Additionally, they have also fostered
71 the revision of the numerical schemes of emissions and deposition, and identified the numerous
72 processes and properties (non-spherical shape of particles, electric forces, atmospheric turbulence),
73 that could counteract the size-selective removal by gravitational settling and keep particles airborne
74 longer than expected (Kok, 2011; Huneus et al., 2011; Mahowald et al., 2011; Kok et al., 2017; Di Biagio
75 et al., 2020; Zhao et al., 2022; Adebisi and Kok, 2020; Adebisi et al., 2020; Huang et al., 2021; Meng et
76 al., 2022; Adeyemi et al., 2023).

77 In support of those activities, in this paper we present a large and standardized compilation of *in situ*
78 observations of the particle size distribution of mineral dust conducted during the past 50 years of
79 research. This dataset extends the currently published ensembles (Meng et al., 2022; Adeyemi et al.,
80 2020; 2023) to provide with a state-of-the art of the current knowledge in support to the development
81 of models, and ground-based and satellite remote sensing. Analysis of this dataset may provide with an
82 integrated view of the size distribution of dust particles across their life cycle to evaluate their impacts
83 in the Earth/human system.

84 2. Methods

85 2.1 Constitution of the dataset

86 Data presented in this paper result from in situ ground-based and aircraft observations of airborne dust
87 conducted during field campaigns during the past 50 years of dust research. Data from deposition
88 samples (e.g., van der Does et al. 2018 or Varga 2021) are not considered in this analysis.

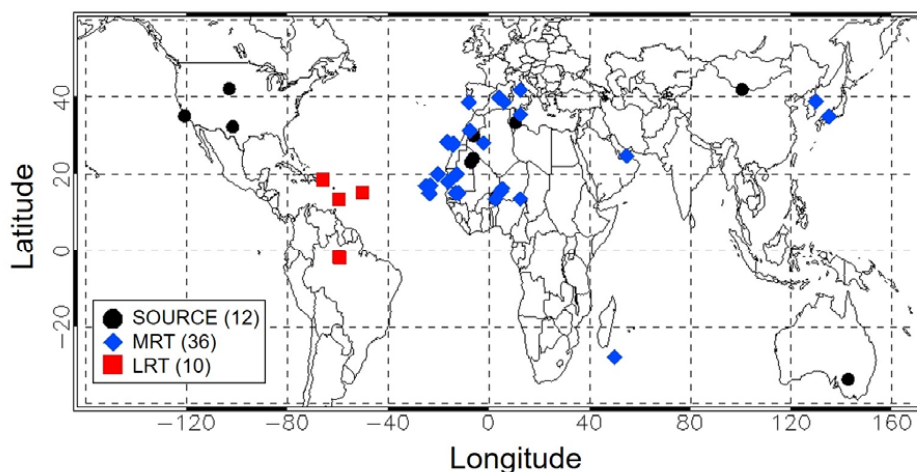
89 Only datasets being published and properly referenced in the open peer-reviewed literature were
90 retained. We also privileged datasets for which the methodology of acquisition, calibration and data



91 treatment was well described so that the data quality can be assessed. Finally, we search for data as
92 much as possible representative of different source and transport regions of the world.

93 The observations contributing to the dataset are listed in **Table S1** and the spelling of the acronyms of
94 the field campaigns is reported in **Text S1** in the supporting material. Data are geo-localized in **Figure 1**,
95 where they are classified with respect to their time after emission.

96
97
98



99
100

101 **Figure 1.** Geographical location of the datasets contributing to size distribution observations for the source, the
102 mid-range transport (MRT) and the long-range transport (LRT) categories. The legend indicates the line style
103 used in the plot. The number of data for each category is indicated in the parenthesis in the legend.

104

105 Observations obtained at the time of dust emission or within 1 day after emission are classified as
106 SOURCE. Observations corresponding to 1 to 4 days after emission and/or geographically acquired
107 near-source regions (for example, offshore North Africa) are classified as mid-range transport (MRT).
108 Observations at times exceeding 4 days after emission or geographically distant from source regions
109 (for example, observations in the Caribbean) are classified as long-range transport (LRT).

110 The SOURCE dataset (Fig 1, black points) consist in 12 observations in Northern Africa, North America,
111 and Asia, and one data point in Australia. They include works by Gillette et al. (1972, 1974), Gillette
112 (1974), Fratini et al. (2007), Rajot et al. (2008), Sow et al. (2009), Shao et al. (2011), Ryder et al. (2013a,
113 2013b), Rosenberg et al. (2014), Huang et al. (2019), and Khalfallah et al. (2020), a set of data recently
114 used by Kok et al. (2017), Di Biagio et al. (2020) and Huang et al. (2021) to constrain the shape of dust
115 size distribution at emission in model studies, and the most recent work by Gonzales-Florez et al. (2023).
116 The MRT class (Fig. 1, blue points) is contributed by 36 datasets from field campaigns (ACE2, ACE-Asia,
117 ADRIMED, AER-D, AMMA, DABEX, DARPO, DIAPASON, DODO1-2, FENNEC, GAMARF, GERBILS, INDOEX,
118 NAMMA, RHaMBLe, SALTRACE, SAMUM1-2, TRACE-P, and UAE2) in Western Africa, Capo Verde, the
119 Mediterranean basin, the eastern tropical Atlantic, Saudi Arabia, Japan, and Indian Ocean, downwind
120 sources either over the ocean or over desert areas. Additional datasets from studies performed in the
121 Sahara, the Atlantic Ocean, Canary Islands and Japan (Schutz, 1981; D’Almeida et al., 1987; Maring et
122 al., 2000; Kobayashi et al., 2007) are added to the dataset. The LRT class (Fig. 1, red points) lays on 10
123 datasets of observations across the Atlantic Ocean and South America and is contributed by
124 observations from Bacex, CLAIRE, Dust-Attack, Go-Amazon, PRIDE, and SALTRACE campaigns and
125 intercontinental dust transport data from Schutz (1981).



126 2.2. Instrumentation contributing to the in situ dataset

127 The natural dynamical range of the particle size and concentration of mineral dust can only be
128 represented by a combination of instruments based on different intrinsic particle properties such as
129 density, electrical charge, shape and composition (e.g., Reid et al., 2003a; Formenti et al., 2011;
130 Wendisch and Brenguier, 2013; Mahowald et al., 2014; Adeyemi et al., 2023). As a consequence, the
131 datasets considered in this paper are contributed by different in situ instruments, also described in **Text**
132 **S2** in the supporting material, namely:

- 133 ○ Optical particle counters (OPC) using the dependence of light scattering on particle size and providing
134 with the particle concentration as a function of the optical equivalent diameter (e.g., Reid et al.,
135 2003b; Clarke et al., 2004; Osborne et al., 2008; Formenti et al., 2011; Ryder et al., 2013a, 2018;
136 Khalfallah et al., 2020).
- 137 ○ Particle collection by filtration or impaction followed by individual particle characterization by
138 transmission (TEM) and/or scanning electron microscopy (SEM) sizing particles as function of their
139 equivalent projected-area diameter and coulter geometric sizing methods, (e.g., Gillette et al., 1972,
140 1974a, 1974b; Reid et al., 2003a; Khobayashi et al., 2007; Kandler et al., 2009; Chou et al., 2008).
- 141 ○ Multi-stage filtration or impaction sampling coupled with gravimetric or chemical analysis providing
142 with the mass size distribution as equivalent aerodynamic diameter (e.g., Formenti et al., 2001; Reid
143 et al., 2003b).
- 144 ○ Differential and Scanning Mobility Particle Sizer (DMPS and SMPS) providing the size of particles in
145 the submicron range as the electrical mobility equivalent diameter of a charged particle moving in a
146 static electric field (e.g., Maring et al., 2000, 2003; Bates et al., 2002; Muller et al., 2010; Denjean et
147 al., 2016a, 2016b).
- 148 ○ Aerodynamic particle sizers (APS), measuring the equivalent aerodynamic diameter of a sphere of
149 unit density having the same terminal velocity in an accelerated airflow as the irregularly shaped
150 dust particles (e.g., Maring et al., 2003; Reid et al., 2003b; 2008; Struckmeier et al., 2016)

151 Each of those instrument types sizes particles on an equivalent diameter (optical, projected-area,
152 aerodynamic, mobility) that depends on their respective working principle. Converting those
153 operational size definitions into a homogenized one is part of the treatment applied in this work, which
154 follows the theory proposed and discussed in the literature and benefits of recent progresses in
155 characterizing/synthesizing dust properties relevant for these treatments (e.g., Hinds, 1999, De Carlo et
156 al., 2004 ; Mahowald et al., 2014; Di Biagio et al., 2019; Huang et al., 2020, 2021; Formenti et al., 2021).
157 Diameter definitions and formulas to convert each of them into a geometrical diameter, both under the
158 assumption of spherical and aspherical dust, is provided in **Text S3** and summarized in **Table S2**.

159 **Text S4** presents relevant information on each dataset considered in the present analysis. This includes
160 a brief description of the field operations, the experimental conditions, the type of original data
161 (number, volume or mass concentration size distribution, size-resolved emission fluxes), the
162 instrumentation, and the data treatment applied to the measurements (averages, diameter corrections,
163 etc.) in the original publication. Original data were obtained, as much as possible, through a personal
164 contact with the data providers or from the original publications based on a digitalization procedure
165 using online tools (<https://automeris.io/WebPlotDigitizer/>). This is also indicated in **Text S4**.

166 2.3. Data treatment, harmonization, and synthesis

167 The original observations were treated to provide with a harmonized dataset both in terms of the
168 definition of particle diameter and differences in number concentrations. Four level of data treatment
169 are defined as described below.

170 1/ *Level-0 (LEVO)*: original data, taken at the native resolution or the resolution from digitalization
171 process and converted into volume distribution assuming spherical particles ($\pi/6 \cdot D^3 \cdot dN/d\log D$), where



172 D is the particle diameter used in the publication and $dN/d\log D$ is the particle number concentration.
173 For starting removing differences due to sampling concentration, and in absence of information on
174 original bin width in the majority of cases, *LEVO* data are normalized so that the maximum of the volume
175 size distribution is equal to 1;

176 2/ *Level-1 (LEV1)*: data from *LEVO* are interpolated over a common size range of equi-logarithmically
177 spaced diameters ($d\log D = 0.05$) encompassing the original diameter range for each dataset and
178 normalized so that the integral is equal to 1 over a common diameter range. The diameter range for
179 integral normalization was set to be the largest as possible and to be covered by more than 90% of the
180 datasets in each category. For *SOURCE* data it resulted that the diameter range for common integral
181 normalization is within 1.58 and 7.1 μm , and for *MRT* and *LRT* it is between 0.71 and 8.9 μm .

182 3/ *Level-2a (LEV2a)*: based on *LEV1*, the *LEV2a* data treatment aims at harmonizing the size distributions
183 by converting the operational original particle diameters, which depend on the physical principle of each
184 instrument, into a common-defined sphere-equivalent geometric diameter. Data from *LEV1* are
185 treated as in the following with respect to their diameter corrections:

- 186 ○ data already provided as geometrical diameters (from coulter counters, i.e. one only dataset in
187 our study) are left unchanged;
- 188 ○ data provided as projected-area diameters (i.e. from microscopy) are left unchanged;
- 189 ○ data provided as aerodynamic diameters (from APS or cascade impactors) are corrected
190 assuming a shape factor (χ) of 1 (under spherical assumption), therefore a size-invariant
191 conversion factor of 1.58 (see Eq. S2) is applied to the dataset assuming dust density of 2.5 g
192 cm^{-3} ($D_{\text{geom}} = D_{\text{aerod}}/1.58$). If original aerodynamic diameter data are already converted into
193 geometrical diameter, we replace the original correction with the conversion factor of 1.58.
194 Since the correction is a multiplicative factor the $d\log D$ of the bins remain unchanged;
- 195 ○ data provided as optical diameters (from OPCs) are converted into sphere-equivalent
196 geometric diameters applying the optical to geometrical correction by assuming homogeneous
197 spherical particles and a value of CRI of 1.53–0.003i. Data for applying the correction for the
198 different model of OPCs considered were taken from Formenti et al. (2021) and conversion
199 factors were recalculated at the $d\log D$ path of 0.05 assumed in the interpolated sizes. For the
200 GRIMM 1.108 for which calibration is not provided in Formenti et al. (2021) we used the data
201 taken from Formenti et al. (2011) (P. Formenti, personal communication) interpolated at the
202 0.05 $d\log D$ path of our diameters. In order to avoid discontinuities appearing and because of
203 the new $d\log D$ do not significantly differ on average from the value of 0.05 for D_{geom} calculated
204 from D_{opt} interpolated data, we do not update the $d\log D$, so that the conversion only imply a
205 shift of the diameter. More details on the choices applied for corrections in different cases are
206 provided in Text S4. Original datasets already converted into geometrical diameter, are left
207 unchanged. However it is worth to note that the ensemble of data already applying an optical
208 to geometrical correction uses a CRI varying between 1.53 and 1.55 for the real part and 0.001
209 and 0.004 for the imaginary part and work under the hypothesis of homogeneous spherical
210 particles (Mie theory), therefore consistent with our treatment. Exceptions are Khalfallah et al.
211 (2020) using a CRI of 1.43–0.00i as for quartz particles, and González-Flórez et al. (2023) using
212 a CRI of 1.49–0.0015i and also applying calculations in ellipsoidal assumption instead of Mie
213 theory. The only dataset not theoretically submitted to the optical to geometric correction is
214 the one provided by Renard et al. (2018) using an OPC built with a specific geometry making the
215 measurements very low sensitive to CRI calibration.

216 4/ *Level-2b (LEV2b)*: based on *LEV1*, the *LEV2b* data treatment aims at harmonizing the size distributions
217 by converting the operational original particle diameters into a common-defined geometrical diameter
218 by taking into account that mineral dust is aspherical. Data from *LEV1* are treated as in the following
219 with respect to their diameter corrections:



- 220 ○ data already provided as geometrical diameters from coulter counters are left unchanged. This
- 221 technique is in fact only slightly affected by shape effects, as discussed by Kobayashi et al.
- 222 (2007);
- 223 ○ data provided as projected–area diameters are corrected using the size–invariant correction
- 224 factor of 1.56 from Huang et al. (2021) ($D_{\text{geom}}=D_{\text{area}}/1.56$) (see Eq. S1);
- 225 ○ data provided as aerodynamic diameter are corrected assuming a size–invariant conversion
- 226 factor of 1.45 following Huang et al. (2021) ($D_{\text{geom}}=D_{\text{aerod}}/1.45$) (see Eq. S2);
- 227 ○ data provided as optical diameters and already treated as for LEV2a data, are further corrected
- 228 by applying a size–dependent aspherical to spherical ratio ($\text{ASR}(D_{\text{geom}})$) correction function,
- 229 $\text{ASR}(D_{\text{geom}})=(D_{\text{geom}})_{\text{aspherical}}/(D_{\text{geom}})_{\text{spherical}}$, to take into account non–sphericity effects in optical to
- 230 geometrical conversion. The ASR function (Fig. S1) is obtained by combining the optical to
- 231 geometrical diameter conversion factors for different OPCs calculated by Formenti et al. (2021)
- 232 and Huang et al. (2021) both in the assumption of spherical homogeneous particles ($(D_{\text{geom}})_{\text{spherical}}$
- 233 and tri–ellipsoids dust ($(D_{\text{geom}})_{\text{aspherical}}$). More details are provided in Text S3. Original datasets
- 234 derived from OPC measurements already provided as geometrical diameter but under
- 235 assumption of sphericity are also corrected by applying the $\text{ASR}(D_{\text{geom}})$ converting function. The
- 236 only exception are González–Flórez et al. (2023), that already apply tri–axial ellipsoids
- 237 calculations in their optical to geometric conversion, and Renard et al. (2018), not requiring
- 238 optical to geometrical conversion.

239 As for LEV1, the LEV2a and LEV2b data, for which a known interpolation path is used, are normalized so
240 that the integral of the volume size distribution is 1 over a common diameter range (1.58 – 7.1 μm for
241 SOURCE, 0.71 – 8.9 μm for MRT, LRT).

242 For each category (SOURCE, MRT, LRT) and for each data level (LEV1, LEV2a, LEV2b), the mean, median,
243 and standard deviation of the particle volume concentration per size class are calculated where at least
244 2 datasets are available in the diameter range. Additionally, the 25% and 75% percentiles are also
245 calculated, despite keeping in mind their limited representativeness given the reduced number of
246 samples in the datasets, especially for SOURCE and LRT classes.

247 2.4. Limitations of the proposed approach

248 Some precisions should be given when considering the LEV2a and LEV2b treatment reported in this
249 work. First, the implicit assumption when applying LEV2a and LEV2b dataset corrections is that dust is
250 the dominant aerosol species and possible effects due to internal or external mixing of dust with other
251 aerosol types are not taken into considerations (i.e., in the complex refractive index or shape factor
252 assumptions). Second, for those datasets that are obtained from the combination of different
253 techniques, namely DMPS+APS (Bates et al., 2002; Maring et al., 2000, 2003; Muller et al., 2010),
254 OPC+APS (Chen et al., 2011), SMPS + OPC (de Reus et al., 2000; Otto et al., 2007; Denjean et al., 2016a,
255 2016b), DMPS + APS + microscopy (Kandler et al., 2011), or multiple OPC instruments (Reid et al., 2003b;
256 McConnell et al., 2008; Johnson and Osborne, 2011; Ryder et al., 2013a, 2013b, 2018; Rosenberg et al.,
257 2014; Weinzierl et al., 2009, 2011, 2017), the choice is that of applying artefact corrections for the
258 dominant instrument, often the one in the extended coarse mode range, and consider this correction
259 applicable to the whole diameter range. This is because when multiples instruments are used to build a
260 size distribution it is then not easy to reconstruct the steps of data analysis and merging from the original
261 work. It follows the subsequent considerations:

- 262 1/ the corrections applied for the aerodynamic and projected–area diameter apply a constant
- 263 size–invariant scaling factor to the ensemble of the size distribution data. In this approximation, if
- 264 the SMPS/DMPS is combined with aerodynamic or microscopy data, a correction factor between
- 265 1.45 and 1.58, depending on the level and the technique as detailed in the previous section, is
- 266 applied in place of the factor 1 (spherical assumption) or 1.19 (aspherical assumption) (see Eq. S3)
- 267 expected to convert the mobility diameter to geometrical diameter in LEV2a and LEV2b data. As a



268 consequence, the submicron size is 20 to 58% finer than expected only due to mobility to geometrical
269 conversion.

270 2/ A similar approach is used to correct datasets where OPC is the main used technique to size dust
271 particles together with the SMPS. For LEV2a data the Mie correction is applied to the full size
272 distribution, but being the size-dependent correction mostly inactive for submicron particles (i.e.
273 $D_{\text{geom}} \sim D_{\text{opt}}$ for most OPCs), the approach is mostly equivalent at considering a mobility diameter
274 correction with a shape factor of 1. For LEV2b data, using OPC corrections induce a limited right
275 shifting of the size distribution compared to the one that would be obtained from mobility
276 conversion because of the magnitude of the ASR function (Fig. S1) compared to the shape factor of
277 1.19 assumed for aspherical dust.

278 3/ When datasets relying on multiple OPCs measurements, the assumption is that the “dominant” OPC
279 that is the OPC covering the largest range and the coarsest sizes in particular, is considered. Given
280 that optical to geometrical corrections are not relevant for submicron particles and that the
281 magnitude of the correction typically increases for increasing sizes, this assumption is not expected
282 to determine significant biases in the data. To mention additionally a general ambiguity of the optical
283 to geometrical correction around the diameter of 1 μm where a plateau in the scattering calibration
284 function for several OPCs models can be found (i.e. Formenti et al., 2021).

285 More details on the specific assumptions and choices done for each dataset are provided in **Text S4**.

286 Further, for LEV2a and LEV2b data for which corrections are applied on the data, caution is take at the
287 boundary of the size distribution and when the first and/or the last bin of the corrected size showed
288 unrealistic divergence, these data are removed from the dataset.

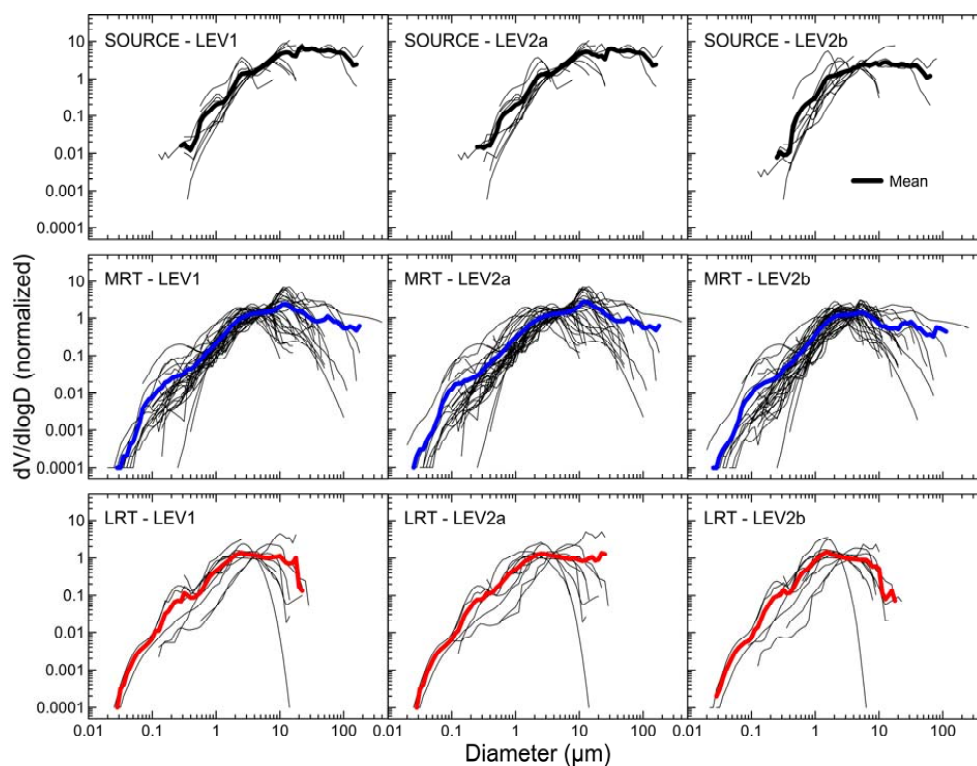
289 3. Presentation and discussion of the dataset

290 Illustration of the data for different levels is provided in Figure 2. Figure 3 presents the synthesis of the
291 LEV2b data and the comparison of SOURCE, MRT and LRT distributions. The contribution of different
292 size classes to the total particle number, surface and volume is summarised in Table 1. Size classes have
293 been defined according to the classification of Adeyemi et al. (2023) defining fine dust ($D \leq 2.5 \mu\text{m}$),
294 coarse dust ($2.5 < D \leq 10 \mu\text{m}$), super coarse dust ($10 < D \leq 62.5 \mu\text{m}$) and giant dust ($D > 62.5 \mu\text{m}$). Within
295 the fine dust class, we further calculate the fractions of particles smaller than 0.4 μm .

296



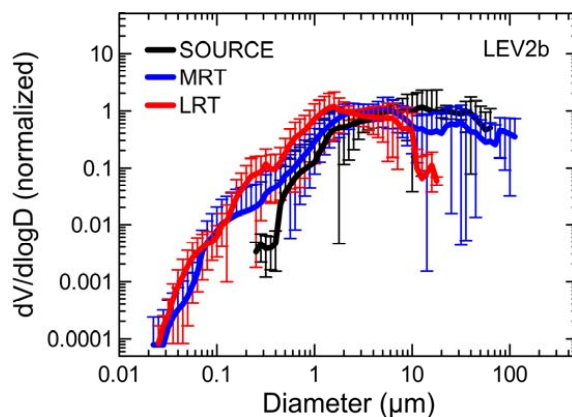
297



298

299 **Figure 2.** Data for SOURCE, MRT, and LRT dust at level 1, 2a, and 2b as described in Sect. 2.3 (labelled as LEV1,
300 LEV2a, LEV2b, respectively). Single datasets, all normalized at the integral of 1, are plotted as black lines. The
301 mean (thick black, blue, and red line for SOURCE, MRT, and LRT, respectively) are shown at all levels. Note that
302 the mean is calculated only where at least 2 datasets are available in the diameter range.

303



304

305 **Figure 3.** Comparison of normalized mean volume size distribution for the SOURCE, MRT, and LRT categories in our study
306 reported as LEV2b data (mean \pm standard deviation). For the sake of comparison, and differently from data in Fig. 2, the
307 SOURCE, MRT, and LRT synthesis datasets reported here are normalized at the integral equal to 1 over a common diameter
308 range corresponding to 0.35–17.8 μm . This is done to remove differences linked to different integration range for SOURCE
309 data compared to MRT and LRT.



310
 311

Dataset		$D \leq 2.5 \mu\text{m}$ ($D \leq 0.4 \mu\text{m}$)	$2.5 < D \leq 10 \mu\text{m}$	$10 < D \leq 62.5 \mu\text{m}$	$D > 62.5 \mu\text{m}$
Number	SOURCE	95.4% (20.4%)	4.5%	0.1%	0.4%
	MRT	99.8% (96.1%)	0.2%	0.0%	0.0%
	LRT	99.9% (94.5%)	0.1%	0.0%	0.0%
Surface	SOURCE	45.0% (1.1%)	39.4%	15.5%	0.14%
	MRT	65.4% (16.8%)	30.7%	3.6%	0.29%
	LRT	84.6% (23.1%)	15.1%	0.2%	0.00%
Volume	SOURCE	10.8% (0.1%)	34.9%	52.7%	1.6%
	MRT	22.1% (1.1%)	44.3%	25.7%	8.0%
	LRT	53.4% (3.6%)	44.5%	2.0%	0.0%

312 **Table 1.** Percentages of number, surface and volume size distribution in the diameter ranges $D \leq 0.4 \mu\text{m}$, $D \leq 2.5 \mu\text{m}$, $2.5 < D \leq$
 313 $10 \mu\text{m}$, $10 < D \leq 62.5 \mu\text{m}$, and $D > 62.5 \mu\text{m}$ for the mean of the size obtained for the SOURCE, MRT, and LRT LEV2b datasets.

314

315 As shown in Fig. 2 and 3 the shape of the dust size distribution at emission and along transport shows
 316 main consistent features. A main mode located at $\sim 10 \mu\text{m}$ (in volume) is observed for dust at emission
 317 and close to sources. The main dust mode decreases to $\sim 5 \mu\text{m}$ and $\sim 2 \mu\text{m}$ for MRT and LRT conditions,
 318 respectively. Below $0.4 \mu\text{m}$ the dust volume size shows an additional mode, particularly visible for MRT
 319 and LRT. As a matter of fact, the sparse datasets measuring very fine particles at the SOURCE show that
 320 particles with diameters below $0.4 \mu\text{m}$ (however measured only down to $0.2 \mu\text{m}$, as shown in Fig. 2)
 321 represent approximately 20% of the total particles' number, increasing to more than 90% in MRT and
 322 LRT. Instruments such as SMPS and DMPS used in MRT and LRT studies measure particles as small as
 323 $0.02 \mu\text{m}$ in diameter. Previous single-particle compositional observations showing that the particle
 324 number concentration in the size range between 0.1 and $0.4 \mu\text{m}$ is largely contributed by aluminosilicate
 325 dust particles at emission, while internal or external mixing with aerosols other than dust gains
 326 importance with time and altitude of transport (Chou et al., 2008; Kandler et al., 2007, 2009; Weinzierl
 327 et al., 2009; 2017; Klaver et al., 2011; Denjean et al., 2016a; 2016b).

328 The size distribution of dust particles between 0.4 and $10 \mu\text{m}$ is rather consistent and invariant along
 329 the dust cycle. This is true in particular when restricting to the 2.5 to $10 \mu\text{m}$ size range when differences
 330 are minimal and contribution to total volume is in between 34.9% and 44.5% . Below that range, which
 331 is between 0.4 and $2.5 \mu\text{m}$, the contribution of particles for LRT is significantly higher (53.4% in volume)
 332 than for SOURCE (10.8%) and MRT (22.1%), likely as, because of the normalization, it compensates the
 333 decrease of particles larger than $10 \mu\text{m}$.

334 The intensity of the particle volume above $10 \mu\text{m}$ remains unchanged almost up to $100 \mu\text{m}$ for both the
 335 SOURCE and the MRT conditions, which also present similar particle volume. This mode decreases very
 336 strongly for LRT conditions, when it represents only 2% of the total volume, compared to almost 55%
 337 and 34% for SOURCE and MRT, respectively.

338 The dataset presented in this work, synthesizing available *in situ* observations, allows to evaluate the
 339 natural variability of dust size distribution along its lifecycle. To be emphasized, however, that while
 340 consistent differences in the mean size distribution curves are obtained going from SOURCE to LRT, as
 341 shown in Fig. 3, the inherent range of variability for each category, represented by the standard
 342 deviation of the data, is also non-negligible and reflects the large range of documented size
 343 distributions, together with the limited statistics available. This is particularly true for both super-coarse
 344 and giant dust at MRT and LRT. Lower variability is identified below $0.4 \mu\text{m}$, but because of the restricted
 345 number of dataset available for MRT and LRT conditions, while we identify an absence of data for
 346 SOURCE dust below this size range.



347 4. Conclusive remark

348 In this paper we present the most possible comprehensive synthesis of *in situ* observations of the
349 particle size distribution of atmospheric dust aerosols. This compilation reflects the current state-of-
350 the-art and represents a standardized and synthetic benchmark to constrain and evaluate models and
351 satellite retrievals. We highlight differences and commonalities of the dust volume distribution as a
352 function of time in the atmosphere, both in terms of main identified modes and relative contribution of
353 dust in different size ranges. A large statistics of data is available and permit to retrieve robust
354 information between 0.4 and 10 μm where most of observations exist, while above and below this size
355 range, observations are rare. Dust particles below 0.4 μm in diameter are seldom measured close to
356 source regions, but are found in observations at mid- and long-range transport conditions. Their
357 presence at emission, their size-segregated composition and state of mixing should be better
358 documented and understood. The dynamics of the coarse mode above 10 μm , its invariance from
359 source to mid-range transport, and decline afterwards is reported, and can challenge models.

360 We acknowledge the evidence that the compilation of a reference dataset is, almost by definition, a
361 subjective and incomplete exercise which must revised continuously with the emergence of new
362 datasets, new field campaigns, and the improvement of sampling techniques. We henceforth encourage
363 colleagues to provide us with new or revised datasets to feed and update the dataset in the future.

364 Data availability

365 The LEV1, LEV2a and LEV2b datasets discussed in this paper are available on the EaSy Data, the Earth
366 System Data repository (<https://www.easydata.earth/#/public/home>, last access: 14 November 2023)
367 maintained by the National French DATA TERRA research Infrastructure. Their respective DOIs are
368 summarized here below:

369 SOURCE_LEV1.dat, SOURCE_LEV2a.dat, SOURCE_LEV2b.dat : <https://doi.org/10.57932/58dbe908-9394-4504-9099-74a3e77140e9> (Formenti and Di Biagio, 2023a);

371 MRT_LEV1.dat, MRT_LEV2a.dat, MRT_LEV2b.dat : <https://doi.org/10.57932/31f2adf7-74fb-48e8-a3ef-059f663c47f1> (Formenti and Di Biagio, 2023b);

373 LRT_LEV1.dat, LRT_LEV2a.dat, LRT_LEV2b.dat : <https://doi.org/10.57932/17dc781c-3e9d-4908-85b5-5c99e68e8f79> (Formenti and Di Biagio, 2023c).

375 Figures of the individual datasets (including LEV0) are provided upon request.

376 **Author contributions.** PF and CDB designed the research, compiled the dataset and analysed it, and
377 wrote the manuscript.

378 **Competing interests.** The authors declare that they have no competing interests.

379 **Special issue statement.** The paper is not associated with a special issue.

380 Acknowledgements

381 PF and CDB acknowledge J. L. Rajot, C. Denjean, A. Adeyemi, D. Meloni, C. Ryder, and J. Kok for providing
382 the original data from their publications. The help of G. Brissebrat to create the DOI for the different
383 datasets is gratefully acknowledged.

384 Funding

385 This research is funded by the project DustClim, part of ERA4CS, an ERA-NET initiated by JPI Climate,
386 and funded by FORMAS (SE), DLR (DE), BMWFW (AT), IFD (DK), MINECO (ES), ANR (FR) with co-funding
387 by the European Union (Grant 690462).



388 References

- 389 Adebisi, A. A., and Kok, J. F.: Climate models miss most of the coarse dust in the atmosphere, *Science Advances*,
390 6, eaaz9507, doi:10.1126/sciadv.aaz9507, 2020.
- 391 Adebisi, A. A., Kok, J. F., Wang, Y., Ito, A., Ridley, D. A., Nabat, P., and Zhao, C.: Dust Constraints from joint
392 Observational–Modelling–experimental analysis (DustCOMM): comparison with measurements and model
393 simulations, *Atmos. Chem. Phys.*, 20, 829–863, <https://doi.org/10.5194/acp-20-829-2020>, 2020.
- 394 Adebisi, A. A., Jasper Kok, Benjamin J Murray, Claire L Ryder, Jan-Berend W Stuut, Ralph A Kahn, Peter Knippertz,
395 Paola Formenti, Natalie M Mahowald, Carlos Pérez García-Pando, Martina Klose, Albert Ansmann, Bjørn Hallvard
396 Samset, Akinori Ito, Yves Balkanski, Claudia Di Biagio, Manolis N Romanias, Yue Huang, and Jun Meng, A review of
397 coarse mineral dust in the Earth system, *Aeolian Research*, 60, <https://doi.org/10.1016/j.aeolia.2022.100849>,
398 2023.
- 399 d’Almeida, G. A.: On the variability of desert aerosol radiative characteristics, 92, 3017–3026,
400 <https://doi.org/10.1029/JD092iD03p03017>, 1987.
- 401 d’Almeida, G. A. and Schütz, L.: Number, Mass and Volume Distributions of Mineral Aerosol and Soils of the Sahara,
402 *J. Climate Appl. Meteor.*, 22, 233–243, [https://doi.org/10.1175/1520-0450\(1983\)022<0233:NMAVDO>2.0.CO;2](https://doi.org/10.1175/1520-0450(1983)022<0233:NMAVDO>2.0.CO;2),
403 1983.
- 404 Bates, T. S., Coffman, D. J., Covert, D. S., and Quinn, P. K.: Regional marine boundary layer aerosol size distributions
405 in the Indian, Atlantic, and Pacific Oceans: A comparison of INDOEX measurements with ACE–1, ACE–2, and
406 Aerosols99, 107, INX2 25–1–INX2 25–15, <https://doi.org/10.1029/2001JD001174>, 2002.
- 407 Baddock, M., Boskovic, L., Strong, C., McTainsh, G., Bullard, J., Agranovski, I., and Cropp, R.: Iron–rich nanoparticles
408 formed by aeolian abrasion of desert dune sand, *Geochemistry, Geophysics, Geosystems*, 14, 3720–3729,
409 <https://doi.org/10.1002/ggge.20229>, 2013.
- 410 Chen, G., Ziemba, L. D., Chu, D. A., Thornhill, K. L., Schuster, G. L., Winstead, E. L., Diskin, G. S., Ferrare, R. A.,
411 Burton, S. P., Ismail, S., Kooi, S. A., Omar, A. H., Slusher, D. L., Kleb, M. M., Reid, J. S., Twohy, C. H., Zhang, H., and
412 Anderson, B. E.: Observations of Saharan dust microphysical and optical properties from the Eastern Atlantic
413 during NAMMA airborne field campaign, 11, 723–740, <https://doi.org/10.5194/acp-11-723-2011>, 2011.
- 414 Chou, C., Formenti, P., Maille, M., Ausset, P., Helas, G., Harrison, M., and Osborne, S.: Size distribution, shape, and
415 composition of mineral dust aerosols collected during the African Monsoon Multidisciplinary Analysis Special
416 Observation Period 0: Dust and Biomass–Burning Experiment field campaign in Niger, January 2006, 113,
417 <https://doi.org/10.1029/2008JD009897>, 2008.
- 418 Claquin, T., Schulz, M., and Balkanski, Y.: Modeling the mineralogy of atmospheric dust sources, *J. Geophys. Res.*,
419 104, 22243–22256, 1999.
- 420 Clarke, A. D., Shinozuka, Y., Kapustin, V. N., Howell, S., Huebert, B., Doherty, S., Anderson, T., Covert, D., Anderson,
421 J., Hua, X., Moore, K. G., McNaughton, C., Carmichael, G., and Weber, R.: Size distributions and mixtures of dust
422 and black carbon aerosol in Asian outflow: Physiochemistry and optical properties, 109,
423 <https://doi.org/10.1029/2003JD004378>, 2004.
- 424 Cuesta, J., Maxim Eremenko, C. Flamant, Gaele Dufour, Benoit Laurent, Gilles Bergametti, M. Hopfner, J. Orphal
425 and D. Zhou, Three-dimensional distribution of a major desert dust outbreak over East Asia in March 2008 derived
426 from IASI satellite observations, *J. Geophys. Res.*, 120, 7099–7127, 2015
- 427 Denjean, C., Formenti, P., Desboeufs, K., Chevaillier, S., Triquet, S., Maillé, M., Cazaunau, M., Laurent, B., Mayol-
428 Bracero, O. L., Vallejo, P., Quiñones, M., Gutierrez-Molina, I. E., Cassola, F., Prati, P., Andrews, E., and Ogren, J.:
429 Size distribution and optical properties of African mineral dust after intercontinental transport, 121, 7117–7138,
430 <https://doi.org/10.1002/2016JD024783>, 2016a.
- 431 Denjean, C., Cassola, F., Mazzino, A., Triquet, S., Chevaillier, S., Grand, N., Bourriane, T., Momboisse, G., Sellegri,
432 K., Schwarzenbock, A., Freney, E., Mallet, M., and Formenti, P.: Size distribution and optical properties of mineral
433 dust aerosols transported in the western Mediterranean, 16, 1081–1104, [https://doi.org/10.5194/acp-16-1081-
434 2016](https://doi.org/10.5194/acp-16-1081-2016), 2016b.



- 435 Di Biagio, C., Y. Balkanski, S. Albani, O. Boucher, and P. Formenti, Direct radiative effect by mineral dust aerosols
436 constrained by new microphysical and spectral optical data, *Geophys. Res. Lett.*, 47, e2019GL086186.
437 <https://doi.org/10.1029/2019GL086186>, 2020.
- 438 Di Biagio, C., Doussin, J. F., Cazaunau, M., Pangu, E., Cuesta, J., Sellitto, P., Rodenas, M., and Formenti, P., Infrared
439 optical signature reveals the source-dependency and along-transport evolution of dust mineralogy as shown by
440 laboratory study, *Sci. Rep.*, 13, 13252, <https://doi.org/10.1038/s41598-023-39336-7>, 2023.
- 441 Dubovik, O., B.N. Holben, T.F. Eck, A. Smirnov, Y.J. Kaufman, M.D. King, D. Tanre, and I. Slutsker (2002), Variability
442 of absorption and optical properties of key aerosol types observed in worldwide locations, *J. Atmos. Sci.*, 59, 590–
443 608, doi:10.1175/1520-0469(2002)059<0590:VOA>.
- 444 Dubovik, O., et al. (2006), Application of spheroid models to account for aerosol particle nonsphericity in remote
445 sensing of desert dust, *J. Geophys. Res.*, 111, D11208, doi:10.1029/2005JD006619.
- 446 Formenti, P., Andreae, M. O., Lange, L., Roberts, G., Cafmeyer, J., Rajta, I., Maenhaut, W., Holben, B. N., Artaxo, P.,
447 and Lelieveld, J.: Saharan dust in Brazil and Suriname during the Large-Scale Biosphere-Atmosphere Experiment
448 in Amazonia (LBA) – Cooperative LBA Regional Experiment (CLAIRE) in March 1998, 106, 14919–14934,
449 <https://doi.org/10.1029/2000JD900827>, 2001.
- 450 Formenti, P., Rajot, J. L., Desboeufs, K., Saïd, F., Grand, N., Chevaillier, S., and Schmechtig, C.: Airborne observations
451 of mineral dust over western Africa in the summer Monsoon season: spatial and vertical variability of physico-
452 chemical and optical properties, 11, 6387–6410, <https://doi.org/10.5194/acp-11-6387-2011>, 2011.
- 453 Formenti, P., Di Biagio, C., Huang, Y., Kok, J., Mallet, M. D., Boulanger, D., and Cazaunau, M.: Look-up tables
454 resolved by complex refractive index to correct particle sizes measured by common research-grade optical
455 particle counters, *Atmos. Meas. Tech. Discuss.* [preprint], <https://doi.org/10.5194/amt-2021-403>, in review,
456 2021.
- 457 Formenti P. and C Di Biagio, Large synthesis of in situ field measurements of the size distribution of mineral dust
458 aerosols across their lifecycle-SOURCE. <https://doi.org/10.57932/58dbe908-9394-4504-9099-74a3e77140e9>,
459 2023a.
- 460 Formenti P. and C Di Biagio, Large synthesis of in situ field measurements of the size distribution of mineral dust
461 aerosols across their lifecycle-MRT. <https://doi.org/10.57932/31f2adf7-74fb-48e8-a3ef-059f663c47f1>, 2023b.
- 462 Formenti P. and C Di Biagio, Large synthesis of in situ field measurements of the size distribution of mineral dust
463 aerosols across their lifecycle-LRT <https://doi.org/10.57932/17dc781c-3e9d-4908-85b5-5c99e68e8f79>, 2023c.
- 464 Fratini, G., Ciccioli, P., Febo, A., Forgiione, A., and Valentini, R.: Size-segregated fluxes of mineral dust from a desert
465 area of northern China by eddy covariance, 7, 2839–2854, <https://doi.org/10.5194/acp-7-2839-2007>, 2007.
- 466 Gillette, D. A., Blifford, I. H., and Fenster, C. R.: Measurements of Aerosol Size Distributions and Vertical Fluxes of
467 Aerosols on Land Subject to Wind Erosion, *J. Appl. Meteor.*, 11, 977–987, [https://doi.org/10.1175/1520-0450\(1972\)011<0977:MOASDA>2.0.CO;2](https://doi.org/10.1175/1520-0450(1972)011<0977:MOASDA>2.0.CO;2), 1972.
- 469 Gillette, D.A. On the production of soil wind erosion having the potential for long range transport, *J. Rech. Atmos.*
470 8, 734–744, 1974.
- 471 Gillette, D. A., Blifford, I. H., and Fryrear, D. W.: The influence of wind velocity on the size distributions of aerosols
472 generated by the wind erosion of soils, 79, 4068–4075, <https://doi.org/10.1029/JC079i027p04068>, 1974.
- 473 Gomes, L., G. Bergametti, G. Coudé-Gaussen, and P. Rognon, Submicron Desert Dusts: A Sandblasting Process, *J.*
474 *Geophys. Res.*, 95 (D9), 927–940, 1990.
- 475 Gómez Maqueo Anaya, S., Althausen, D., Faust, M., Baars, H., Heinold, B., Hofer, J., Tegen, I., Ansmann, A.,
476 Engelmann, R., Skupin, A., Heese, B., and Schepanski, K.: The implementation of dust mineralogy in COSMO5.05-
477 MUSCAT, EGU sphere [preprint], <https://doi.org/10.5194/egusphere-2023-1558>, 2023
- 478 González-Flórez, C., Klose, M., Alastuey, A., Dupont, S., Escibano, J., Etyemezian, V., Gonzalez-Romero, A., Huang,
479 Y., Kandler, K., Nikolich, G., Panta, A., Querol, X., Reche, C., Yus-Díez, J., and Pérez García-Pando, C.: Insights into
480 the size-resolved dust emission from field measurements in the Moroccan Sahara, *Atmos. Chem. Phys.*, 23, 7177–
481 7212, <https://doi.org/10.5194/acp-23-7177-2023>, 2023.



- 482 Gonçalves Ageitos, M., V. Obiso, R.L. Miller, O. Jorba, M. Klose, M. Dawson, Y. Balkanski, J. Perlwitz, S. Basart, E. Di
483 Tomaso, J. Escribano, F. Macchia, G. Montané, N. Mahowald, R.O. Green, D.R. Thompson, and C. Pérez García-
484 Pando, 2023: Modeling dust mineralogical composition: sensitivity to soil mineralogy atlases and their expected
485 climate impacts. *Atmos. Chem. Phys.*, **23**, no. 15, 8623–8657, doi:10.5194/acp-23-8623-2023.
- 486 Green, R. O. *et al.* The earth surface mineral dust source investigation: an earth science imaging spectroscopy
487 mission. in: *2020 IEEE Aerospace Conference* 1–15 (2020). <https://doi.org/10.1109/AERO47225.2020.9172731>.
- 489 Huang, Y., Kok, J. F., Martin, R. L., Swet, N., Katra, I., Gill, T. E., Reynolds, R. L., and Freire, L. S.: Fine dust emissions
490 from active sands at coastal Oceano Dunes, California, 19, 2947–2964, [https://doi.org/10.5194/acp-19-2947-](https://doi.org/10.5194/acp-19-2947-2019)
491 2019, 2019.
- 492 Huang, Y., Adebijiy, A. A., Formenti, P., & Kok, J. F., Linking the different diameter types of aspherical desert dust
493 indicates that models underestimate coarse dust emission. *Geophys. Res. Lett.*, **48**, e2020GL092054,
494 <https://doi.org/10.1029/2020GL092054>, 2021.
- 495 Huneus, N., Schulz, M., Balkanski, Y., Griesfeller, J., Prospero, J., Kinne, S., Bauer, S., Boucher, O., Chin, M.,
496 Dentener, F., Diehl, T., Easter, R., Fillmore, D., Ghan, S., Ginoux, P., Grini, A., Horowitz, L., Koch, D., Krol, M. C.,
497 Landing, W., Liu, X., Mahowald, N., Miller, R., Morcrette, J.-J., Myhre, G., Penner, J., Perlwitz, J., Stier, P., Takemura,
498 T., and Zender, C. S.: Global dust model intercomparison in AeroCom phase I, *Atmos. Chem. Phys.*, **11**, 7781–7816,
499 <https://doi.org/10.5194/acp-11-7781-2011>, 2011.
- 500 Johnson, B. T. and Osborne, S. R.: Physical and optical properties of mineral dust aerosol measured by aircraft
501 during the GERBILS campaign, **137**, 1117–1130, <https://doi.org/10.1002/qj.777>, 2011.
- 502 Journet, E., Balkanski, Y., and Harrison, S. P.: A new data set of soil mineralogy for dust-cycle modeling, *Atmos.*
503 *Chem. Phys.*, **14**, 3801–3816, <https://doi.org/10.5194/acp-14-3801-2014>, 2014.
- 504 Jung, E., Albrecht, B., Prospero, J. M., Jonsson, H. H., and Kreidenweis, S. M.: Vertical structure of aerosols,
505 temperature, and moisture associated with an intense African dust event observed over the eastern Caribbean,
506 *Journal of Geophysical Research: Atmospheres*, **118**, 4623–4643, <https://doi.org/10.1002/jgrd.50352>, 2013.
- 507 Kaaden, N., Massling, A., Schladitz, A., Müller, T., Kandler, K., Schütz, L., Weinzierl, B., Petzold, A., Tesche, M.,
508 Leinert, S., Deutscher, C., Ebert, M., Weinbruch, S., and Wiedensohler, A.: State of mixing, shape factor, number
509 size distribution, and hygroscopic growth of the Saharan anthropogenic and mineral dust aerosol at Tinfou,
510 Morocco, **61**, 51–63, <https://doi.org/10.1111/j.1600-0889.2008.00388.x>, 2009.
- 511 Kandler, K., Schütz, L., Deutscher, C., Ebert, M., Hofmann, H., JäCKEL, S., Jaenicke, R., Knippertz, P., Lieke, K.,
512 Massling, A., Petzold, A., Schladitz, A., Weinzierl, B., Wiedensohler, A., Zorn, S., and Weinbruch, S.: Size
513 distribution, mass concentration, chemical and mineralogical composition and derived optical parameters of the
514 boundary layer aerosol at Tinfou, Morocco, during SAMUM 2006, **61**, 32–50, [https://doi.org/10.1111/j.1600-](https://doi.org/10.1111/j.1600-0889.2008.00385.x)
515 0889.2008.00385.x, 2009.
- 516 Kandler, K., Schütz, L., Jäckel, S., Lieke, K., Emmel, C., Müller–Ebert, D., Ebert, M., Scheuvsens, D., Schladitz, A.,
517 Šegvić, B., Wiedensohler, A., and Weinbruch, S.: Ground–based off–line aerosol measurements at Praia, Cape
518 Verde, during the Saharan Mineral Dust Experiment: microphysical properties and mineralogy, **63**, 459–474,
519 <https://doi.org/10.1111/j.1600-0889.2011.00546.x>, 2011.
- 520 Khalfallah, B., Bouet, C., Labiadh, M. T., Alfaro, S. C., Bergametti, G., Marticorena, B., Lafon, S., Chevaillier, S., Féron,
521 A., Hease, P., Tureaux, T. H. des, Sekrafi, S., Zapf, P., and Rajot, J. L.: Influence of Atmospheric Stability on the Size
522 Distribution of the Vertical Dust Flux Measured in Eroding Conditions Over a Flat Bare Sandy Field, **125**,
523 e2019JD031185, <https://doi.org/10.1029/2019JD031185>, 2020.
- 524 Knippertz, P. and Stuut, J.-B. W. (Eds.): *Mineral Dust: A Key Player in the Earth System*, Springer Netherlands,
525 <https://doi.org/10.1007/978-94-017-8978-3>, 2014.
- 526 Kobayashi, H., Arao, K., Murayama, T., Iokibe, K., Koga, R., and Shiobara, M.: High–Resolution Measurement of Size
527 Distributions of Asian Dust Using a Coulter Multisizer, *J. Atmos. Oceanic Technol.*, **24**, 194–205,
528 <https://doi.org/10.1175/JTECH1965.1>, 2007.
- 529 Kok JF (2011) A scaling theory for the size distribution of emitted dust aerosols suggests climate models
530 underestimate the size of the global dust cycle. *Proc Natl Acad Sci U S A* **108**:1016–1021



- 531 Kok, J. F., Ridley, D. A., Zhou, Q., Miller, R. L., Zhao, C., Heald, C. L., Ward, D. S., Albani, S., and Haustein, K.: Smaller
532 desert dust cooling effect estimated from analysis of dust size and abundance, 10, 274–278,
533 <https://doi.org/10.1038/ngeo2912>, 2017.
- 534 Mahowald, N., Lindsay, K., Rothenberg, D., Doney, S. C., Moore, J. K., Thornton, P., Randerson, J. T., and Jones, C.
535 D.: Desert dust and anthropogenic aerosol interactions in the Community Climate System Model coupled-carbon-
536 climate model, *Biogeosciences*, 8, 387–414, <https://doi.org/10.5194/bg-8-387-2011>, 2011.
- 537 Maring, H., Savoie, D. L., Izaguirre, M. A., McCormick, C., Arimoto, R., Prospero, J. M., and Pilinis, C.: Aerosol
538 physical and optical properties and their relationship to aerosol composition in the free troposphere at Izaña,
539 Tenerife, Canary Islands, during July 1995, 105, 14677–14700, <https://doi.org/10.1029/2000JD900106>, 2000.
- 540 Maring, H., Savoie, D. L., Izaguirre, M. A., Custals, L., and Reid, J. S.: Mineral dust aerosol size distribution change
541 during atmospheric transport, 108, <https://doi.org/10.1029/2002JD002536>, 2003.
- 542 McConnell, C. L., Highwood, E. J., Coe, H., Formenti, P., Anderson, B., Osborne, S., Nava, S., Desboeufs, K., Chen,
543 G., and Harrison, M. a. J.: Seasonal variations of the physical and optical characteristics of Saharan dust: Results
544 from the Dust Outflow and Deposition to the Ocean (DODO) experiment, 113,
545 <https://doi.org/10.1029/2007JD009606>, 2008.
- 546 Meloni, D., Junkermann, W., Sarra, A. di, Cacciani, M., Silvestri, L. D., Iorio, T. D., Estellés, V., Gómez-Amo, J. L.,
547 Pace, G., and Sferlazzo, D. M.: Altitude-resolved shortwave and longwave radiative effects of desert dust in the
548 Mediterranean during the GAMARF campaign: Indications of a net daily cooling in the dust layer, 120, 3386–3407,
549 <https://doi.org/10.1002/2014JD022312>, 2015.
- 550 Meng, J., Huang, Y., Leung, D. M., Li, L., Adebisi, A. A., Ryder, C. L., Mahowald, N. M., and Kok, J. F.: Improved
551 Parameterization for the Size Distribution of Emitted Dust Aerosols Reduces Model Underestimation of Super
552 Coarse Dust, *Geophysical Research Letters*, 49, e2021GL097287, <https://doi.org/10.1029/2021GL097287>, 2022.
- 553 Menut, L., Siour, G., Bessagnet, B., Couvidat, F., Journet, E., Balkanski, Y., and Desboeufs, K.: Modelling the
554 mineralogical composition and solubility of mineral dust in the Mediterranean area with CHIMERE 2017r4, *Geosci.*
555 *Model Dev.*, 13, 2051–2071, <https://doi.org/10.5194/gmd-13-2051-2020>, 2020.
- 556 Müller, K., Lehmann, S., van Pinxteren, D., Gnauk, T., Niedermeier, N., Wiedensohler, A., and Herrmann, H.: Particle
557 characterization at the Cape Verde atmospheric observatory during the 2007 RHaMBLe intensive, 10, 2709–2721,
558 <https://doi.org/10.5194/acp-10-2709-2010>, 2010.
- 559 Osborne, S. R., Johnson, B. T., Haywood, J. M., Baran, A. J., Harrison, M. a. J., and McConnell, C. L.: Physical and
560 optical properties of mineral dust aerosol during the Dust and Biomass-burning Experiment, 113,
561 <https://doi.org/10.1029/2007JD009551>, 2008.
- 562 Otto, S., de Reus, M., Trautmann, T., Thomas, A., Wendisch, M., and Borrmann, S.: Atmospheric radiative effects
563 of an in situ measured Saharan dust plume and the role of large particles, 7, 4887–4903,
564 <https://doi.org/10.5194/acp-7-4887-2007>, 2007.
- 565 Perlwitz, J.P., C. Pérez García-Pando, and R.L. Miller: Predicting the mineral composition of dust aerosols — Part
566 1: Representing key processes. *Atmos. Chem. Phys.*, 15, 11593–11627, doi:10.5194/acp-15-11593-2015, 2015a.
- 567 Perlwitz, J.P., C. Pérez García-Pando, and R.L. Miller: Predicting the mineral composition of dust aerosols — Part
568 2: Model evaluation and identification of key processes with observations. *Atmos. Chem. Phys.*, 15, 11629–11652,
569 doi:10.5194/acp-15-11629-2015, 2015b.
- 570 Rajot, J. L., Formenti, P., Alfaro, S., Desboeufs, K., Chevaillier, S., Chatenet, B., Gaudichet, A., Journet, E.,
571 Marticorena, B., Triquet, S., Maman, A., Mouget, N., and Zakou, A.: AMMA dust experiment: An overview of
572 measurements performed during the dry season special observation period (SOP0) at the Banizoumbou (Niger)
573 supersite, 113, <https://doi.org/10.1029/2008JD009906>, 2008.
- 574 Reid, E. A., Reid, J. S., Meier, M. M., Dunlap, M. R., Cliff, S. S., Broumas, A., Perry, K., and Maring, H.:
575 Characterization of African dust transported to Puerto Rico by individual particle and size segregated bulk analysis,
576 108, <https://doi.org/10.1029/2002JD002935>, 2003a.
- 577 Reid, J. S., Jonsson, H. H., Maring, H. B., Smirnov, A., Savoie, D. L., Cliff, S. S., Reid, E. A., Livingston, J. M., Meier, M.
578 M., Dubovik, O., and Tsay, S.-C.: Comparison of size and morphological measurements of coarse mode dust
579 particles from Africa, 108, <https://doi.org/10.1029/2002JD002485>, 2003b.



- 580 Reid, J. S., Reid, E. A., Walker, A., Piketh, S., Cliff, S., Mandoos, A. A., Tsay, S.-C., and Eck, T. F.: Dynamics of
581 southwest Asian dust particle size characteristics with implications for global dust research, 113,
582 <https://doi.org/10.1029/2007JD009752>, 2008.
- 583 Renard, J.-B., Dulac, F., Durand, P., Bourgeois, Q., Denjean, C., Vignelles, D., Couté, B., Jeannot, M., Verdier, N.,
584 and Mallet, M.: In situ measurements of desert dust particles above the western Mediterranean Sea with the
585 balloon-borne Light Optical Aerosol Counter/sizer (LOAC) during the ChArMEx campaign of summer 2013, 18,
586 3677–3699, <https://doi.org/10.5194/acp-18-3677-2018>, 2018.
- 587 de Reus, M., Dentener, F., Thomas, A., Borrmann, S., Ström, J., and Lelieveld, J.: Airborne observations of dust
588 aerosol over the North Atlantic Ocean during ACE 2: Indications for heterogeneous ozone destruction, 105, 15263–
589 15275, <https://doi.org/10.1029/2000JD900164>, 2000.
- 590 Rosenberg, P. D., Dean, A. R., Williams, P. I., Dorsey, J. R., Minikin, A., Pickering, M. A., and Petzold, A.: Particle
591 sizing calibration with refractive index correction for light scattering optical particle counters and impacts upon
592 PCASP and CDP data collected during the Fennec campaign, 5, 1147–1163, <https://doi.org/10.5194/amt-5-1147-2012>, 2012.
- 594 Rosenberg, P. D., Parker, D. J., Ryder, C. L., Marsham, J. H., Garcia-Carreras, L., Dorsey, J. R., Brooks, I. M., Dean, A.
595 R., Crosier, J., McQuaid, J. B., and Washington, R.: Quantifying particle size and turbulent scale dependence of dust
596 flux in the Sahara using aircraft measurements, 119, 7577–7598, <https://doi.org/10.1002/2013JD021255>, 2014.
- 597 Ryder, C. L., Highwood, E. J., Lai, T. M., Sodemann, H., and Marsham, J. H.: Impact of atmospheric transport on the
598 evolution of microphysical and optical properties of Saharan dust, 40, 2433–2438,
599 <https://doi.org/10.1002/grl.50482>, 2013a.
- 600 Ryder, C. L., Highwood, E. J., Rosenberg, P. D., Trembath, J., Brooke, J. K., Bart, M., Dean, A., Crosier, J., Dorsey, J.,
601 Brindley, H., Banks, J., Marsham, J. H., McQuaid, J. B., Sodemann, H., and Washington, R.: Optical properties of
602 Saharan dust aerosol and contribution from the coarse mode as measured during the Fennec 2011 aircraft
603 campaign, 13, 303–325, <https://doi.org/10.5194/acp-13-303-2013>, 2013b.
- 604 Ryder, C. L., Marengo, F., Brooke, J. K., Estelles, V., Cotton, R., Formenti, P., McQuaid, J. B., Price, H. C., Liu, D.,
605 Ausset, P., Rosenberg, P. D., Taylor, J. W., Choularton, T., Bower, K., Coe, H., Gallagher, M., Crosier, J., Lloyd, G.,
606 Highwood, E. J., and Murray, B. J.: Coarse-mode mineral dust size distributions, composition and optical properties
607 from AER-D aircraft measurements over the tropical eastern Atlantic, 18, 17225–17257,
608 <https://doi.org/10.5194/acp-18-17225-2018>, 2018.
- 609 Scanza, R. A., Mahowald, N., Ghan, S., Zender, C. S., Kok, J. F., Liu, X., Zhang, Y., and Albani, S.: Modeling dust as
610 component minerals in the Community Atmosphere Model: development of framework and impact on radiative
611 forcing, *Atmos. Chem. Phys.*, 15, 537–561, <https://doi.org/10.5194/acp-15-537-2015>, 2015.
- 612 Schladitz, A., Müller, T., Nowak, A., Kandler, K., Lieke, K., Massling, A., and Wiedensohler, A.: In situ aerosol
613 characterization at Cape Verde, 63, 531–548, <https://doi.org/10.1111/j.1600-0889.2011.00569.x>, 2011.
- 614 Schütz, L. and Jaenicke, R.: Particle Number and Mass Distributions above 10–4 cm Radius in Sand and Aerosol of
615 the Sahara Desert, *J. Appl. Meteor.*, 13, 863–870, [https://doi.org/10.1175/1520-0450\(1974\)013<0863:PNAMDA>2.0.CO;2](https://doi.org/10.1175/1520-0450(1974)013<0863:PNAMDA>2.0.CO;2), 1974.
- 617 Schütz, L., Jaenicke, R., and Pietrek, H.: Saharan dust transport over the North Atlantic Ocean,
618 <https://doi.org/10.1130/SPE186-p87>, 1981.
- 619 Shao, Y., Ishizuka, M., Mikami, M., and Leys, J. F.: Parameterization of size-resolved dust emission and validation
620 with measurements, 116, <https://doi.org/10.1029/2010JD014527>, 2011.
- 621 Sow, M., Alfaro, S. C., Rajot, J. L., and Marticorena, B.: Size resolved dust emission fluxes measured in Niger during
622 3 dust storms of the AMMA experiment, 9, 3881–3891, <https://doi.org/10.5194/acp-9-3881-2009>, 2009.
- 623 Struckmeier, C., Drewnick, F., Fachinger, F., Gobbi, G. P., and Borrmann, S.: Atmospheric aerosols in Rome, Italy:
624 sources, dynamics and spatial variations during two seasons, 16, 15277–15299, <https://doi.org/10.5194/acp-16-15277-2016>, 2016.
- 626 Sviridenkov, M. A., Gillette, D. A., Isakov, A. A., Sokolik, I. N., Smirnov, V. V., Belan, B. D., Pachenko, M. V.,
627 Andronova, A. V., Kolomiets, S. M., Zhukov, V. M., and Zhukovsky, D. A.: Size distributions of dust aerosol measured



- 628 during the Soviet–American experiment in Tadzhikistan, 1989, *Atmospheric Environment. Part A. General Topics*,
629 27, 2481–2486, [https://doi.org/10.1016/0960-1686\(93\)90019-U](https://doi.org/10.1016/0960-1686(93)90019-U), 1993.
- 630 Wagner, F., Bortoli, D., Pereira, S., Costa, M. Jo., Silva, A. M., Weinzierl, B., Esselborn, M., Petzold, A., Rasp, K.,
631 Heinold, B., and Tegen, I.: Properties of dust aerosol particles transported to Portugal from the Sahara desert, 61,
632 297–306, <https://doi.org/10.1111/j.1600-0889.2008.00393.x>, 2009.
- 633 Walser, A., Sauer, D., Spanu, A., Gasteiger, J., and Weinzierl, B.: On the parametrization of optical particle counter
634 response including instrument–induced broadening of size spectra and a self–consistent evaluation of calibration
635 measurements, 10, 4341–4361, <https://doi.org/10.5194/amt-10-4341-2017>, 2017.
- 636 Weinzierl, B., Petzold, A., Esselborn, M., Wirth, M., Rasp, K., Kandler, K., Schütz, L., Koepke, P., and Fiebig, M.:
637 Airborne measurements of dust layer properties, particle size distribution and mixing state of Saharan dust during
638 SAMUM 2006, 61, 96–117, <https://doi.org/10.1111/j.1600-0889.2008.00392.x>, 2009.
- 639 Weinzierl, B., Sauer, D., Esselborn, M., Petzold, A., Veira, A., Rose, M., Mund, S., Wirth, M., Ansmann, A., Tesche,
640 M., Gross, S., and Freudenthaler, V.: Microphysical and optical properties of dust and tropical biomass burning
641 aerosol layers in the Cape Verde region—an overview of the airborne in situ and lidar measurements during
642 SAMUM-2, 63, 589–618, <https://doi.org/10.1111/j.1600-0889.2011.00566.x>, 2011.
- 643 Weinzierl, B., Ansmann, A., Prospero, J. M., Althausen, D., Benker, N., Chouza, F., Dollner, M., Farrell, D., Fomba,
644 W. K., Freudenthaler, V., Gasteiger, J., Groß, S., Haarig, M., Heinold, B., Kandler, K., Kristensen, T. B., Mayol-
645 Bracero, O. L., Müller, T., Reitebuch, O., Sauer, D., Schäfler, A., Schepanski, K., Spanu, A., Tegen, I., Toledano, C.,
646 and Walser, A.: The Saharan Aerosol Long–Range Transport and Aerosol–Cloud–Interaction Experiment: Overview
647 and Selected Highlights, *Bull. Amer. Meteor. Soc.*, 98, 1427–1451, <https://doi.org/10.1175/BAMS-D-15-00142.1>,
648 2017.
- 649 Zhao, A., Ryder, C. L., and Wilcox, L. J.: How well do the CMIP6 models simulate dust aerosols?, *Atmos. Chem.*
650 *Phys.*, 22, 2095–2119, <https://doi.org/10.5194/acp-22-2095-2022>, 2022.
- 651 Zhou, Y., R. C. Levy, et al. "Dust Aerosol Retrieval over the Oceans with the MODIS/VIIRS Dark Target algorithm.
652 Part I: Dust Detection." *Earth and Space Science* n/a(n/a): e2020EA001221.